The internal flow properties of a vertical submersible axial flow pump device were studied, and the structure was optimize

Dr. Ravi naik[1], S.Pavan Kalyan[2], CH Sushma[3],

[1,2,3] *Assistant Professor Department of mechanical St.Martin's Engineering College Secunderabad, Telangana, India.*

Abstract

The steady and unsteady three-dimensional numerical simulation of a vertical submersible axial-flow pump device was carried out based on CFD in order to investigate the internal flow characteristics and hydraulic stability of the pump station in forward and reverse operation, and the energy performance of the pump device was predicted. The internal flow characteristics of the vertical submersible axial-flow pump device were examined in this study under forward and reverse operation, and the structure passed by water was optimized to improve the pump device's efficiency in forward and reverse operation. The results reveal that the pump device's performance is good when it is running forward, and that the pump device's peak efficiency is high.

Keywords

Submersible axial flow pump, flow conduit, internal flow characteristics, structural optimization, bidirectional operation, numerical simulation

1. INTRODUCTION

benefits of achieving urban flood management requirements and increasing the performance of the urban river water environment At the moment, certain established urban vertical axial flow pumping stations must be converted from one-way to bidirectional pumping. However, a significant amount of civil engineering investment in the restoration of vertical pumping stations is required. The adjustment in hydraulic structure also pre-embed safety threats for the pumping station's safe and stable operation in the future. It is practical and cost-effective to employ the S-shaped reversible impeller to accomplish the reverse pumping function of the pumping station with only minor changes to the original one-way flow conduit. Mudu's modified pump device, for example Figure 1. Three-dimensional model of vertical Figure . Main

geometric dimensions of conduit: (a) dust-pan-shaped flow conduit and (b) wellbore flow conduit.

Introduction

vertical submersible axial flow pump in bidirectional mode, it is important to investigate the internal flow mechanism of the device. The hydraulic performance of a vertical submersible axial flow pump device was anticipated using a numerical simulation method in this research, and the internal flow properties of each flow structure in forward and reverse operation were investigated. The flow structure of the pump device is optimized as a consequence of the study, providing a reference for the optimization design and efficient, safe, and stable operation of a vertical submerged axial flow pump device.The homogeneous flow assumption and an alternate truncated Rayleigh-Plesset equation The effect of tip clearance on pressure variations in an axial flow water pump was studied by Jianjun Feng et al.9. Kan et al.10 investigated the improvement of dynamic stress in an axialflow pump and confirmed the simulation results with a prototype test. Kan et al.11 investigated the spinning stall flow characteristics of an axial-flow pump using 3D computational fluid dynamics (CFD). Lin et al.12 used the computational fluid dynamics (CFD) method to evaluate the effect of silt on cavitation in an axial-flow pump's internal flow field.

Figure 2 mechanism under various conditions.

Pump device model and calculation technique
Model and parameters for calculation
The vertical submerged axial flow pump device is made up of four flow passage components: a dust-pan-shaped flow conduit, a reversible impeller, a guide vane, and a vertical submersible axial flow pump device.

2. Model and calculation method of pump

as well as a wellbore flow conduit Figure 1 depicts a three-dimensional representation of the pump device. The reversible impeller has a "S" wing shape to it. The impeller has three blades, the blade placement angle is 0°, the hub ratio is 0.4, the impeller tip clearance is 0.1 mm, the impeller speed is 1450 r/min, the guide vane is a diffusion guide vane, the equivalent diffusion angle of water flow in the guide vane is 10°, and the guide vane has five blades. According to the nominal diameter
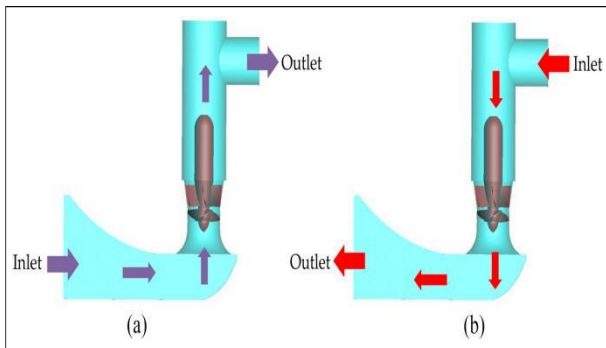
Figure 3. Bidirectional operation diagram of pump device: (a) forward operation and (b) reverse operation.

shown in Figure 3(a). When the vertical submersible axial flow pump device runs reversely, the water reverses through the impeller to work from the well- bore flow conduit into the dust-pan-shaped flow con- duit, and the operation mode is shown in Figure 3(b).

3. Numerical methods and boundary conditions

The medium provided by the vertical submersible axial flow pump device is an incompressible liquid, and the flow in the pump device is a three-dimensional unstable turbulent flow that follows the governing equations of the N-S equation. 26 In this study, the RNG k-e model is used to numerically simulate the pump device, which can better deal with flows with high strain rates and large streamline curvature. The turbulent model has shown to be quite helpful in modelling the flow field in pumps and pump equipment. 27–29 The mass flow inlet boundary condition is employed at the inlet of the dust-pan-shaped flow conduit extension section, and the pressure outlet is used. belong to the interface that is static. There
ICEM CFD structured meshes the dust-pan-shaped flow conduit and the wellbore flow conduit. The three-dimensional models of the dust-pan-shaped flow conduit and the wellbore flow conduit are imported into the ICEM CFD software, and each component is identified. The

created block corresponds to each part of the model until the block approximation geometric model is established. The

consistency of the model and the created block structure is assured by mapping the relationship between points, lines, and surfaces, and the O-Block operation is performed on the built block to ensure the quality of the model's wall boundary layer grid. Ansys Turbo-Grid divides the impeller and guiding vane into structured grids, andflow pump device is analyzed. By adjusting the number of structured grid nodes to continuously increase the
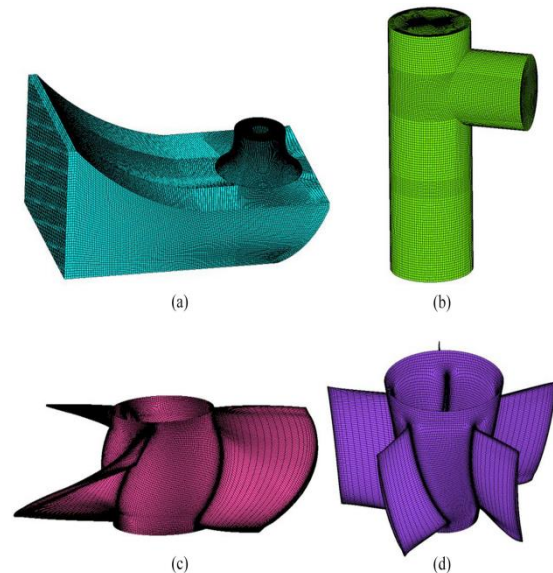
Figure 4. Wall grid diagram of vertical submersible axial flow pump device: (a) dust-pan-shaped flow conduit, (b) wellbore flow conduit, (c) impeller, and (d) guide vane.

The number of grids received is 1523455, 2234480, 3129080, 4003213, 5443241, and 8093453, and the grid numbers are 1523455, 2234480, 3129080, 4003213, 5443241, and 8093453, respectively. 1–6 are the grid cal- culation systems that correlate. The pump device efficiency and the absolute difference between pump device efficiency are used to determine the grid's logic. The grid number is suitable when the pump device efficiency changes little and the absolute difference between the pump device efficiency is minor. Figure 5 depicts the findings of the analysis.
Pump device efficiency is calculated using the absolute difference formula:

Where ha is the absolute difference in pump device efficiency, I j is the mesh number, I = 1,2,..., 5, j = I + 1, and ha is the absolute difference in pump device efficiency.
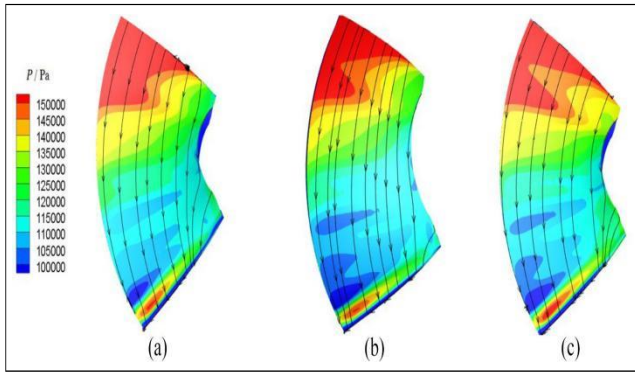
Ity requirements.8,12

Figure 5
The grid convergence index GCI (Grid

Figure 6. Pump device efficiency curve with different numbers of grids and efficiency difference.

Figure 7. Pump device energy performance curve (forward operation).
Flow line and pressure distribution of dust-pan-shaped flow conduit (forward operation): (a) KQ = 0.490, (b) KQ = 0.536, and (c) KQ = 0.583.

disordered, and the swirling flow is generated at the top of the conduit.

Internal flow characteristics in a forward-flow dust-pan-shaped flow conduit are investigated. The dispersion of the flow field at the exit of the dust-pan-shaped flow conduit has a significant impact on the impeller's operation efficiency. Figure 9 depicts the streamlines and pressure contours of the dust-pan-shaped flow conduit's center longitudinal section under three flow conditions. Under various flow conditions, the pressure distribution inside the dust-pan-shaped flow conduit steadily drops from the input to the outlet. When the flow rate is increased, the pressure inside the dustpan-shaped flow conduit increases as well. The pressure is symmetrically distributed at the output surface of the dust-pan-shaped flow conduit, and the velocity distribution is rather homogeneous. The internal streamline of the internal streamline of the internal streamline of the internal streamline of the internal streamline of the internal streamline of the

0.536, and (c) KQ = 0.583.

Figure 8. The friction line and contours of pressure on the pressure surface of the impeller (forward operation): (a) KQ = 036, and (c) KQ = 0.583.

. The friction line and contours of pressure on the suction surface of the impeller (forward operation): (a) KQ = 0.490, (b) KQ = 0.536, and (c) KQ = 0.583

 Three-dimensional flow field diffusion guide vane (forward operation): (a) KQ = 0.490, (b) KQ = 0.536, and (c) KQ = 0.583.
). The friction line and contours of pressure on the impeller suction surface are shown in Figure 11. The friction line of the impeller blade suc- tion surface is relatively straight. The pressure of the blade suction surface increases from the inlet side to the outlet side under different flow conditions, and the impeller blade suction surface increases with the increase of flow rate.
The three-dimensional flow field inside the diffuser guide vane under different flow conditions is shown in Figure 12. Under each flow condition, the flow line

4. Analysis of hydraulic performance parameters of pump device

inside the guide vane is relatively straight as a whole. Due to the difference in the flow velocity part under each flow condition, the vortex and backflow appear on the back of the guide vane. Under the small flow condi- tion (KQ = 0.490), the vortex range on the back of the guide vane is large. Under the high efficiency condition (KQ = 0.536), the vortex is significantly reduced. Under the large flow condition (KQ = 0.583), the vortex on the back of the guide vane completely disappears, mainly because the velocity circulation at the impeller outlet is small under the large flow condition and the influence

Figure 13. Flow line and pressure contours of wellbore flow channel (forward operation): (a) KQ = 0.490, (b) KQ =
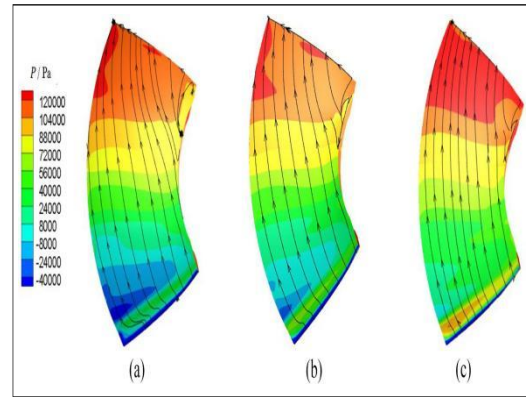
Figure 9 Internal flow line of pump device (reverse operation): (a) KQ = 0.322, (b) KQ = 0.368, and (c) KQ = 0.414.
city on the mainstream is wea- kened, which leads to smooth streamline in the guide vane.

The flow characteristics of a positive inflow wellbore flow conduit. The streamline and pressure contours of a well-bore flow conduit are shown in Figure 13. Under various flow conditions, the pressure inside the wellbore flow conduit gradually rises from the bottom to the top of the conduit, and the pressure at the top of the conduit gradually lowers to the conduit's exit. The pressure at the top of the wellbore flow conduit is at its highest, while the pressure below the exit pipe is at its lowest. Under varied flow circumstances, the streamline distribution inside the well- bore flow conduit is chaotic, and the streamline inside the flow conduit gradually becomes straight as the flow rate increases. There are several alternatives to choose from.
Examination of opposite stream qualities of siphon gadget
Interior stream examination is done in the opposite activity of the upward sub pivotal stream siphon gadget under the little stream condition (KQ = 0.322), the high productivity condition (KQ = 0.368), and the huge stream condition (KQ = 0.414). Figure 14 portrays the general stream line chart of the upward sub pivotal stream siphon gadget under three different stream conditions. Under various stream conditions, the smooth out morphological characteristics inside the bay and outlet channels are equivalent. The liquid enters the wellbore through the result line of the borewell stream channel, making a huge scope vortex structure around the liquid, and the smooth out thickness on the left half of the wellbore stream course is significantly higher.

5. Flow conduit structure optimization analysis

Flow line and pressure distribution of dustpan-shaped flow conduit (reverse operation): (a) KQ = 0.322, (b) KQ = 0.368 and (c) KQ = 0.414.r, it very well may be seen from the smooth out shape underneath the impeller that the liquid has a huge speed circula-tion and an enormous speed. At the point when it enters the lower part of the residue container formed stream channel, the effect happens, and a huge scope of vortexes are dispersed in the entire stream field. What's more, the smooth out bit by bit will in general be directly from the lower part of the impeller to the delta of the residue skillet formed stream conductor.

Investigation of inside stream attributes of converse activity dust-skillet molded stream course. It tends to be seen from Figure 15 that when the siphon gadget is backward activity, the tension appropriation in the residue dish formed stream conductor changes minimal under various stream conditions. Under various stream conditions, the strain changes in the locale beneath the impeller in the conductor are huge, and the tension qualities in different districts are comparative. The vortex place at the impeller outlet is a low-pressure locale, and the high-pressure district is for the most part distribu-ted on the course divider. The smooth out dispersion in the residue skillet molded stream course is extremely scattered. At each stream condition, vortices are shaped close to the water guide cap, and a huge scope reverse zone is framed beneath the impeller, and the stream design is poor.

Inside stream qualities of impeller and guide vane in turn around activity. In switch activity, the functioning substance of impeller cutting edge is inverse to that in forward show tion. As displayed in Figure 16, there is little distinction in the strain dispersion of the attractions surface of the impeller sharp edge under three different stream conditions. The strain at the bay side of the edge is the most minimal

under a similar stream condition, and the strain increments step by step from the delta side to the power source side of the sharp edge. With the increment of stream rate, the surface strain of edge attractions surface steadily increments. The erosion lines on the pull surface of impeller cutting edge are generally straight, yet there is an incomplete stream peculiarity on the contact line at the center of sharp edge outlet edge, and the more modest the stream rate is, the more clear the halfway stream peculiarity is. The strain dispersion of impeller sharp edge pressure surface is displayed in Figure 17. The strain at the channel edge of impeller sharp edge pressure surface steadily diminishes from the spine to the center point, and the tension step by

step diminishes from the gulf edge to the power source edge. The tension dis-tribution of the strain surface of the cutting edge under dif-ferent stream conditions is clearly divergent in the neighborhood. There is an enormous low tension region close to the power source edge of the cutting edge

under little stream condition and huge stream condition, and the strain at the center point of the edge under little stream condition is bigger. There are various levels of reverse on the tension surface of the impeller cutting edge. The more modest the stream rate, the more clear the discharge on the cutting edge surface.

The three-layered stream field of the aide vane is displayed in Figure 18. In switch activity, the aide vane is changed from back to front, and the speed cir-culation of the liquid can't be recuperated, and the liquid is more scattered because of the impact of the curve on the rear of the aide vane. Taking into account the unique situa-tion of the redirection brought about by the difference in the origi-nal wellbore stream conductor into the gulf stream channel, the front aide vane actually affects the liquid. The three-layered stream field
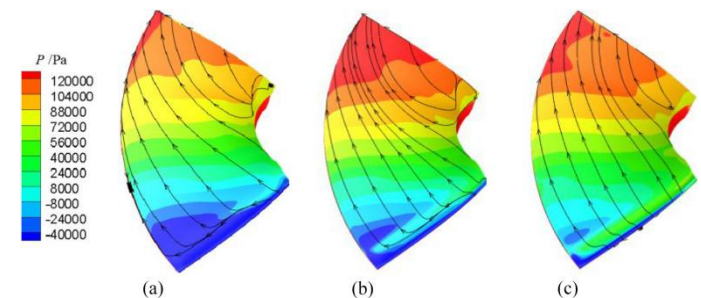

Figure 10. The friction line and contours of pressure on the suction surface of the impeller (reverse operation): (a) KQ = 0.322, (b) KQ = 0.368, and (c) KQ = 0.414.
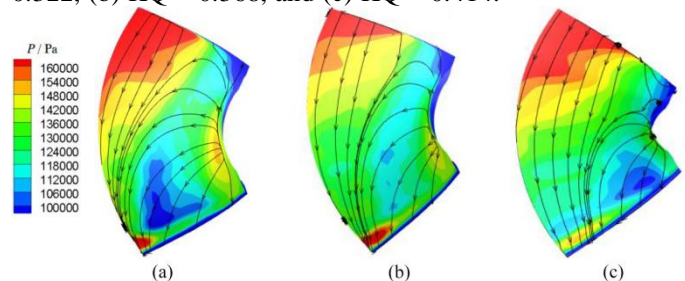

Figure 11. The friction line and contours of pressure on the pressure surface of the impeller (reverse operation): (a) KQ = 0.322, (b) KQ = 0.368 and (c) KQ = 0.414.
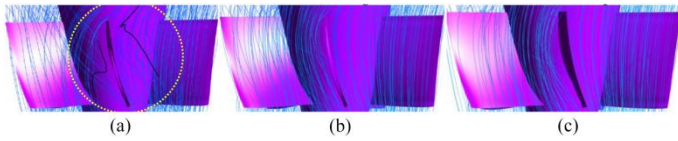
Figure 12. Three-dimensional flow field diffusion guide vane (reverse operation): (a) KQ = 0.322, (b) KQ = 0.368 and (c) KQ = 0.414.

guide vane is obtained by post-processing. It is observed that the streamline distribution at the guide vane is similar under different flow conditions, which is more uniform and no backflow phenomenon. When the streamline enters the guide vane from above, the deflection is obvi- ous, and the guide vane blade has certain improvement.Flow characteristics of reverse inflow wellbore flow conduit. The flow line and pressure contour of reverse operation wellbore flow conduit are shown as Figure 19. The pressure distribution of the wellbore flow conduit under different flow conditions shows that the pressure from the water pipe to the top of the wellbore increases gradually, and the pressure from the top to the bottom

Figure 19. Flow line and pressure contour of wellbore flow channel (reverse operation): (a) KQ = 0.322, (b) KQ = 0.368 and (c) KQ = 0.414.
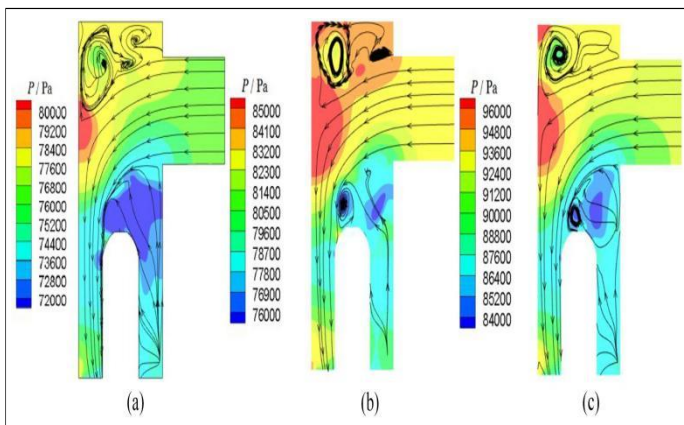
Figure 13
ity distribution uniformity and velocity weighted average angle (forward operation).
Flow coefficient Axial velocity distribution uniformity/(%)
    Velocity weighted average angle/(°)

B are greater than section A-A underue to the effect of circulation, the flow pattern in the flow conduit is not good, which seriously affects the perfor- mance of the pump device. In order to explore the cir- culation changes in the outlet flow conduit under different flow conditions, when the pump device is run- ning forward, three sections are selected in the wellbore flow conduit to calculate the

average velocity circula- tion. When the pump device is running backward, two sections at the impeller outlet and below the flare tube are selected in the dust-pan-shaped flow conduit to cal- culate the average velocity circulation.32 The calcula- tion of the average velocity circulation is shown in formula (4). The schematic diagram of the section is shown in Figure 21. The impeller inlet section D-D is selected, and the distance between section E-E and D- D is D; the impeller outlet section A-A is selected, the distance between section B-B and A-A is 0.9D, and the distance between section C-C and A-A is 1.9D; the D- D distance of impeller centerline to section is 0.15D.d hub

boundary of
1. Characteristic section position diagram: (a) forward operation and (b) reverse operation.
Figure 22. Average velocity circulation of wellbore flow conduit (forward operation). Figure 23. Average velocity circulation of dust-pan-shaped flow conduit (reverse operation).

It can be seen from Figure 22 that when the flow condition is KQ = 0.322, the average velocity circula- tion of section A-A reaches the maximum value, and the average velocity circulation decreases with the increase of flow rate. At the same time, the farther away from the impeller, the smaller the average velocity circulation is. Figure 23 shows the average velocity cir- culation of the dust-pan-shaped flow conduit under the reverse operation of the pump device. Under the reverse operation of the pump device, the flow rate under the high efficiency condition is less than that under the for- ward operation, and there is no recovery of the velocity circulation by the guide vane, resulting in a large circu- lation at the outlet of the impeller. When the flow coef- ficient is 0.32, the average velocity circulation of the section D-D reaches the maximum value, which is 1.54 times that under the forward operation. This is because
rea below the flare tube is large, resulting in a relatively small average velocity circulation.

Analysis of hydraulic loss. In order to further analyze the variation of hydraulic loss under different flow condi- tions, the hydraulic loss ratio K is defined as the ratio of hydraulic loss to pump device head. In forward operation, dust-pan-shaped flow conduit is the inlet flow conduit, and wellbore flow conduit is the outlet flow conduit; in reverse operation, the dustpan-shaped flow conduit is the outflow flow conduit, and the well- bore flow conduit is the inlet flow conduit. The hydrau- lic loss of the dustpan-shaped channel and the wellbore flow conduit is shown in Figure 24. The hydraulic loss of the dust-pan-shaped flow conduit increases with the increase of the flow rate, and the change is more regu- lar. The hydraulic loss of wellbore flow conduit increases with the increase of flow rate. The hydraulic

ead loss. When the flow rate is small, the circulation loss accounts for a large proportion. When the flow rate is large, the flow rate increases, and the frictional head loss and local head loss increase. There is a large range of backflow area

annihilate. The vortex band is mainly concentrated in the

loss is large. The wellbore flow conduit has a great influence on the overall effi- ciency of the pump device. In the range of flow coeffi- cient KQ = 0.460–0.613, the hydraulic loss ratio of the wellbore flow conduit is the lowest 12.0% and the high- est 43.83%. In the reverse operation of the pump device, the hydraulic loss is similar to that in the for- ward operation, but the hydraulic performance is poor, and the hydraulic loss is significantly greater than that in the forward operation. In addition, the proportion of hydraulic loss in the dust-pan-shaped flow conduit increases with the increase of flow rate.

vicinity of the inlet of the dust-pan-shaped flow conduit, and the vortex band is basically disappeared
nduit should be mainly aimed at the area below the impeller.

Internal vortex morphology evolution of pump device outlet structure. When the vertical submersible axial flow pump device runs in the positive direction, the fluid still has a large circulation after flowing through the guide vane. The structural characteristics of the top of the wellbore make a large number of vortexes in the region and inside the outlet pipe. In the identification method of vortex morphology, there are mainly pressure isosur-

face method, Q criterion and l2 criterion, O vortex cri- terion and Liutex vortex vector method. Q criterion and l2 criterion have stronger ability to capture vortex morphology comparatively, and can clearly and rea-

sonably display vortex morphology, so as to capture the internal flow characteristics and the development

gy in the water pipe more intuitively. In this study, based on the Q criterion, the threshold value of Q is set to 1000 s22, and the vor- tex pattern of the wellbore flow conduit at the charac- teristic time in a rotating period T of the impeller of the pump device under the high efficiency condition (KQ = 0.536) is shown in Figure 25. The vortex belt is mainly distributed at the top and bottom of the well- bore. The vorticity is large at the outlet pipe of the well- bore flow conduit, and the flow velocity is also significantly improved. It can be seen that due to the difference in the diameter of the wellbore outlet pipe, the increase in the flow velocity after the fluid flows into the outlet pipe from the wellbore leads to fluid dis- order and the increase in the vorticity, which is one of the main reasons for the flow pattern difference in the wellbore flow conduit.

When the pump device runs in reverse, the dust-pan- shaped flow conduit is below the impeller, and the fluid has a large circulation after flowing out of the impeller, and the flow rate is large, which is easy to form rotary vortex. The threshold of Q is also selected as 1000 s22. Based on the Q criterion, the vortex structure of the dust-pan-shaped flow conduit in a rotating cycle of the impeller during the reverse operation of the pump device is drawn as Figure 26. The vortex band is mainly concentrated in the inlet of the dust-pan-shaped flow conduit, and the flow rate is large. The vortex spreads into the low part of the dust-pan-shaped flow conduit and begins to disappear. Some vortex bands directly hit the bottom of the dust-pan-shaped flow conduit and then

Flow conduit structure optimization analysis
Optimization strategy analysis of wellbore flow conduit
The wellbore flow conduit structure has an adverse effect on the flow state during forward and reverse operation. During forward operation, there is a back- flow zone at the top corner of the wellbore, and the backflow zone is at the junction of the wellbore and the water outlet pipe. A low pressure zone is formed at the inlet of the water outlet pipe, and there are a large number of vortex bands. In the reverse

operation of the pump device, when the fluid flows into the wellbore from the outlet pipe, a large-scale vortex is formed on both sides of the fluid space, which increases the hydraulic loss.
w conduit is controlled to be 3.33D, the diameter is 1.35D, the motor length is 1.37D, and the diameter is 0.58D (D is the nominal diameter of the impeller), which is consistent with that of the wellbore flow conduit. By taking five horizontal values within the angle range for three-dimensional modeling and numerical simulation analysis of the pump device, the influence of elbow channel angle radius R on the per- formance of the pump device is explored (Table 4).
The calculation formula of device efficiency varia- tion in the table is:

Dh = h0 — hb   ð5Þ

Where Dh is the change value of device efficiency, h0 is the pump device efficiency of the elbow flow conduit, hb is the pump device efficiency of wellbore flow conduit.
According to Table 5, it is known that different cor- ner radius has some influence on the hydraulic perfor- mance of the pump device. When the pump device is
raulic loss of the outlet flow conduit decreases. When the corner radius is 1.33D, the effi- ciency of the pump device reaches the highest. When the pump device runs in the reverse direction, the maxi- mum efficiency of the pump device is 41.13%, and the corner radius is 0.83D. Since the corner radius R has little effect on the performance of the pump device in
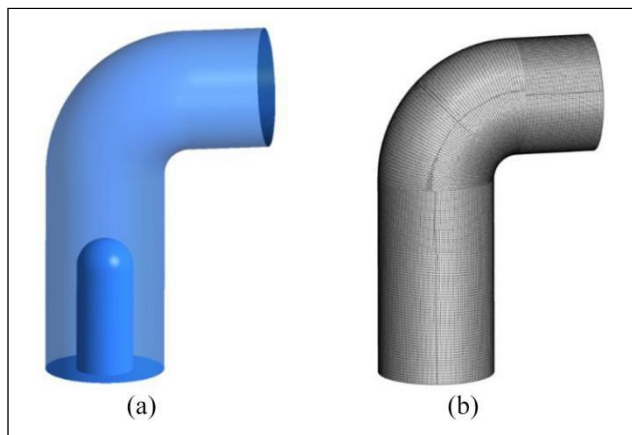
Figure 14. Elbow flow conduit and model grid: (a) three-dimensional model and (b) model grid.

siphon gadget, the framework number of the elbow stream con-duit is controlled to be essentially predictable with that of the first wellbore stream channel. The elbow stream con-duit is displayed in Figure 27.

The three-layered consistent mathematical reproduction of vertical submarine pivotal stream siphon gadget is done by supplanting the wellbore stream conductor with the elbow

stream channel. The stream line and tension con-voyages through the elbow stream channel of the vertical submersi-ble pivotal stream siphon gadget are gotten when the siphon gadget is running in forward activity and opposite activity (Figure 28). At the point when the siphon gadget is run-ning forward, because of the impact of the engine, the bowing and twist of the stream line close to the engine in the elbow stream course is more not kidding. Likewise, the liquid in the elbow stream course has enormous dissemination, so the smooth out close to the inward mass of the channel has slight bowing and twist, yet there is no vortex in the conductor. At the point when the siphon gadget runs conversely, the stream line inside the conductor is straight and the tension

dispersion is uniform, and there is no terrible stream design inside the channel.

In view of the Q standard, the vortex state inside the power source construction of the siphon gadget is recognized. The edge of Q is changed in accordance with 1000 s22, and the noticeable Figure 29 of the vortex state of the power source structure under the positive and converse activity conditions is gotten. It tends to be seen from Figure 29 that in the for-ward activity of the siphon gadget, contrasted and the first wellbore stream course (Figure 25), the vortex morphology in the stream channel changes extraordinarily in the wake of changing to the elbow stream conductor. At the lower part of the elbow stream conductor, the vortex band brought

about by the flow is fundamentally decreased and the conveyance is generally uniform. At the highest point of the elbow stream channel, the vortex stream speed is more uniform. At the point when the siphon gadget works in the converse bearing, after the elbow stream channel is taken on, the vortex band inside the residue skillet molded stream conductor is not exactly that in the first gadget (Figure 26), the divider appended vortex of the flare tube divider is diminished, the twisting vortex band in the cylinder is more self-evident, and the vortex band gathered nearby beneath the flare tube is altogether decreased.

Enhancement procedure and investigation of residue container molded course

At the point when the upward submarine hub stream siphon gadget runs in the forward heading, the stream line inside the stream conductor is smooth and the water powered execution is great. The antagonistic stream design primarily happens in the wellbore stream conductor. At the point when the siphon gadget runs in the converse bearing, the stream design in the dustpan-molded stream channel and the wellbore stream course is generally poor. By utilizing the elbow stream channel to supplant the wellbore stream channel, the unfavorable stream pat-tern of the siphon gadget in the forward course is basi-cally vanished. The primary justification for the low

Flow line and pressure contours of the elbow flow conduit: (a) forward operation and (b) reverse operation.

Vortex diagram in outlet structure of pump device: (a) forward operation – elbow flow conduit and (b) reverse operation – dust-pan-shaped flow conduit.n reverse operation is the disorder of the internal flow pattern of the dustpan- shaped flow conduit. Since the internal flow pattern of the dust-pan-shaped flow conduit is similar to that of the turbine draft tube, the performance of the reverse operation device of the pump device is improved by set-ting the guide plate inside the dust-pan-shaped flow conduit.

Influence of guide plate on pump device performance. Referring to the research results of previ- ous scholars,33,34 by setting the guide plate in the draft tube axis to affect the vortex band below the impeller, the impact on the pipe wall can be weakened to achieve the optimization effect. Due to the small height of the dust-pan-shaped flow conduit in this device, the fluid still has great kinetic energy and circulation after flow- ing out of the impeller and reaching the bottom of the flow conduit, so it is impossible to determine the best installation position of the guide plate. The shaping line of the guide plate is set according to the streamline, so it is not appropriate to change the position of the guide plate on the Z axis (pump axis). This study attempts to increase the width of the guide plate to make it closer to the impeller to strengthen the diversion effect of the guide plate. After numerical simulation verification, it is concluded that due to the excessive circulation of the fluid after flowing out of the

impeller in reducing the width of the guide plate will aggravate the impact of the fluid on the guide plate, thereby reducing the effi- ciency of the device.

The position of the guide plate on the X-axis will affect its diversion effect on the fluid flowing out of the impeller. Assuming that the impeller axis is located at the coordinate origin on the x-axis, it is positive to the right (Figure 30). Seven horizontal values are set at the position of the guide plate in the x-axis direction, which are 20.10D, 0D, 0.13D, 0.27D, 0.40D, 0.53D, and

0.6pec
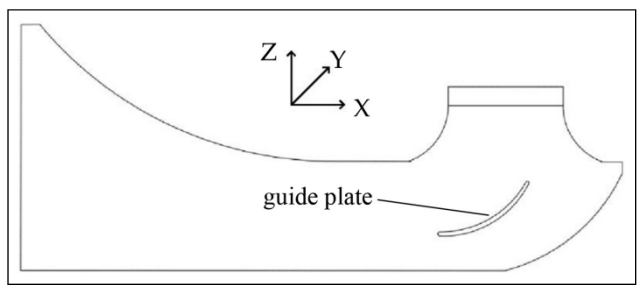
Figure 15 Setting of guide plate.

numerical simulation, the pump device performance under high-efficiency flow conditions in forward and reverse operation is obtained, as shown in Table 5.

The calculation formula of device efficiency change in the table is:

$$Dh = h0 - hb \quad ð6Þ$$

Where Dh is the change value of device efficiency, h0 is to set the guide plate after the pump device efficiency, hb is

the device efficiency without guide plate.

Table 5 shows that in the forward operation, the

greater the deviation from the initial position of the guide plate, the stronger the flow disturbance effect, the lower the efficiency of the pump device, and the

ases with the increase of x. In the reverse operation, the device effi- ciency reaches the maximum when X is 0.27D, and the device head is the highest and the hydraulic loss of the flow conduit is the smallest. The medians of 0.20D and 0.40D in the adjacent interval of 0.27D are taken for three-dimensional modeling and numerical simulation. Compared with the device performance of x = 0.27D, it can be seen from Table 4 that 0.27D is the optimal position of the guide plate scheme. The end of the guide plate near the inlet of the dust-pan-shaped flow conduit is 20.62D on the X axis. The two ends of the Z axis of the guide plate are 1.3D and 0.83D away from the outlet surface of the dust-pan-shaped flow conduit.

Analysis of flow field and vortex state in the conduit after

add- ing guide plate. After installing the guide plate in the dust-pan-shaped flow conduit, carry out the simulation

calculation of the constant constant value of the vertical submersible axial flow pump device. The set- ting method and grid of the deflector are shown in Figure 31. The internal streamline and pressure con- tours of the dust-pan-shaped flow conduit of the verti- cal submersible axial flow pump device under the forward and reverse operation of the pump device under standard working conditions are obtained

Dust-pan-shaped flow conduit and grid diagram with guide plate: (a) three-dimensional model and (b) model grid.

shaped flow conduit: (a) forward operation and (b) reverse operation.

agram in outlet structure of pump device: (a) forward operation – elbow flow conduit and (b) reverse operation – dust-pan-shaped flow conduit.

(Figure 32), and the internal flow pattern of the dust- pan-shaped flow conduit without guide plate is com- pared (Figures 9 and 15). It can be seen that when the pump device is running forward, the setting of guide plate has little impact on the internal flow of the inlet conduit, there is no adverse flow pattern such as vortex in the inlet conduit, and the streamline and pressure distribution are similar to those without guide plate. When the pump device runs in the reverse direction, there are still a large number of vortices in the internal wall area of the dust-pan-shaped flow conduit, and the flow pattern is disordered. However, compared with the internal flow pattern of the conduit

without guide plate under the same flow condition, due to the influ- ence of the guide plate, the large-scale vortex at the bottom of the dust-pan-shaped flow conduit becomes a smaller wall attached vortex, and the pressure distribu- tion in the conduit is more uniform, and the flow pat- tern is

improved on the whole.

Based on the Q criterion, the vortex structure of dust-pan-shaped flow conduit and elbow flow conduit with guide plate under high-efficiency working condi- tions (forward KQ = 0.536, reverse K = 0.368) during forward and reverse operation is identified. As shown in Figure 33, the vortex structure in elbow flow conduit is not significantly different from that without guide plate (Figure 25). After setting guide plate, the vorticity at the bottom of the dust-pan-shaped flow conduit increases, and the vorticity at the top

and in the outlet pipe decreases. During the reverse operation of the pump device, compared with the original internal vortex band shape (Figure 26), it can be seen that the setting of the guide plate has a great impact on the internal vortex band of the dust-pan-shaped flow con- duit. In Figure 33, there is mainly a thick spiral vortex band under the impeller, which is very similar to the vortex band shape in the draft tube of the hydraulic turbine, In the original installation, it may be because the fluid has a wide range of longitudinal whirlingwaters at the bottom of the flow conduit, which inter- feres with the vortex structure in the horn tube, making the wall attached vortex more obvious in the horn tube.

6. Conclusion

The energy performance of vertical submersible axial flow pump device during forward and reverse operation is predicted, the internal flow characteristics of each overflow structure are analyzed, and the structural opti- mization and hydraulic analysis of dust-pan-shaped flow conduit and wellbore flow conduit are carried out. The conclusions are as follows:

The hydraulic performance of the pump device is good in the forward operation. The maximum efficiency of the pump device is 72.22%, and the corresponding head is 4.01 m (KQ = 0.430). The flow pattern in the inlet conduit of the pump device is good, and the pressure distribu- tion is uniform. There is a part of vortex in the guide vane inside the back of the guide vane. With the increase of flow rate, the vortex becomes smaller, but there are many vortexes in the elbow flow conduit, which have a great influence on the pump device. In the reverse operation, the performance of the pump device decreased significantly, the maximum efficiency was only 36.03%, and the corresponding head was 3.34 m. The inlet conditions of the wellbore flow

conduit were poor, and most of the back- flow areas existed in the internal, and the partial flow phenomenon was serious. The convection state of the front guide vane was improved. In the dust-pan-shaped flow conduit, the fluid velocity

In the forward operation, the hydraulic loss in the dust-pan-shaped flow conduit is very small. Under the high efficiency condition (KQ = 0.536), the uniformity of axial velocity distribution at the impeller inlet is 83.06%, and the maximum weighted average angle of velo- city is 78.31°. However, the wellbore flow con- duit affects the

performance hydraulic loss of the device, and the maximum hydraulic loss ratio is 43.83%. In the reverse operation, the hydraulic loss in the wellbore flow conduit is large. In the high efficiency condition (KQ = 0.368), the uniformity of axial velocity distribution at the outlet of the wellbore flow conduit is 67.24%, and the minimum weighted average

angle is 66.40°. After the flow passes through the guide vane, the uniformity of axial velocity distribution increases to 72.25%, and the weighted average angle of velocity increases to 74.80°. Based on the Q criterion, the vortex pattern inside the outlet conduit is captured. In the forward operation, the vortex band is mainly distributed at the inlet of the wellbore flow conduit and the top of the wellbore and the outlet of the outlet pipe. In the reverse oper- ation, the vortex band inside the dust-pan- shaped flow conduit is mainly concentrated in the horn tube.

The wellbore flow conduit is changed into the elbow flow conduit. When the corner radius is set to 0.83D, the efficiency of the pump device increases by 6.13% in the forward operation and 5.10% in the reverse operation. On the basis of adopting the elbow flow channel, set- ting the guide plate inside the dustpan-shaped flow channel can reduce the vortex inside the dustpan-shaped flow conduit, which can improve the efficiency of the pump device by 3.52% in reverse operation.

7. References

Meng F, Li Y, Yuan S, et al. Effect of hub clearance on hydraulic performance in bidirectional axial-flow pump. Trans Chin Soc Agric Mach 2020; 51: 131–138.

Wang W, Wang W, Zhang L, et al. Mechanism for end- wall slots to improve hump in an axial flow pump. Trans Chin Soc Agric Eng 2020; 36: 12–20.

Yu H, Fan Z, Wallace et al. Orthogonal optimum design method for high specific-speed axial-flow pumps. Journal of Vibration and Shock 2018; 37: 115–121.

Zhang H, Zuo F, Zhang D, et al. Formation and evolu- tion mechanism of tip leakage vortex in axial flow pump and vortex cavitation analysis. Chin Soc Agric Mach 2021; 52: 157–167.

Zhao W, Zhao F and Lu J. Study on the control of cavi- tation of axial flow pump with discontinuous bulges on the back of blades. J Eng Thermophys 2021; 42: 96–105.

Chen E, Ma Z, Zhao G, et al. Numerical investigation on vibration and noise induced by unsteady flow in an axial-flow pump. J Mech Sci Technol 2016; 30: 5397–5404.

Dai J, Liu X, Huang C, et al. Experiment on pressure pulsation of axial flow pump system with different run- away head. Processes 2021; 9: 1597.

Feng H, Wan Y and Fan Z. Numerical investigation of turbulent cavitating flow in an axial flow pump using a new transport-based model. J Mech Sci Technol 2020; 34: 745–756.

Feng J, Luo X, Guo P, et al. Influence of tip clearance on pressure fluctuations in an axial flow pump. J Mech Sci Technol 2016; 30: 1603–1610.

Kan K, Zheng Y, Chen H, et al. Study into the improve- ment of dynamic stress characteristics and prototype test of an impeller blade of an axial-flow pump based on bidirectional fluid–structure interaction. Appl Sci 2019; 9: 3601.

Kan K, Zheng Y, Chen Y, et al. Numerical study on the internal flow characteristics of an axial-flow pump under stall conditions. J Mech Sci Technol 2018; 32: 4683–4695.

Lin P, Hu D, Lu JM, et al. CFD numerical simulation of sand-contained cavitation characteristics of axial-flow pump. Adv Mech Eng 2021; 13: 16878140211032784.

Mu T, Zhang R, Xu H, et al. Study on improvement of hydraulic performance and internal flow pattern of the axial flow pump by groove flow control technology. Renew Energy 2020; 160: 756–769.

Shen S, Qian Z and Ji B. Numerical analysis of mechani- cal energy dissipation for an axial-flow pump based on entropy generation theory. Energies 2019; 12: 4162.

Shervani-Tabar MT, Ettefagh MM, Lotfan S, et al. Cavi- tation intensity monitoring in an axial flow pump based on vibration signals using multi-class support 018; 232: 3013–3026.

Shi L, Zhang W, Jiao H, et al. Numerical simulation and experimental study on the comparison of the hydraulic characteristics of an axial-flow pump and a full tubular pump. Renew Energy 2020; 153: 1455–1464.

Song X and Liu C. Experimental investigation of pressure pulsation induced by the floor-attached vortex in an axial flow pump. Adv Mech Eng 2019; 11: 1687814019838708.

Svoboda DG, Zharkovskii AA, Ivanov EA, et al. High-efficiency axial pumps for reactor use. Russ Eng Res 2019; 39: 556–560.

Yang F, Chang P, Hu W, et al. Numerical study on pres- sure pulsation in a slanted axial-flow pump device under partial loads. Processes 2021; 9: 1404.

Yang F, Li Z, Yuan Y, et al. Numerical and experimental investigation of internal flow characteristics and pressure fluctuation in inlet passage of axial flow pump under deflection flow conditions. Energies 2021; 14: 5245.

Yang F, Zhang Y, Yuan Y, et al. Numerical and experi- mental analysis of flow and pulsation in hump section of siphon outlet conduit of axial flow pump device. Appl Sci 2021; 11: 4941.

Zhang D, Shi L, Zhao R, et al. Study on unsteady tip leakage vortex cavitation in an axial-flow pump using an improved filter-based model. J Mech Sci Technol 2017; 31: 659–667.

Zhang W, Shi L, Tang F, et al. Analysis of inlet flow pas- sage conditions and their influence on the performance of an axial-flow pump. Proc IMechE, Part A: J Power and Energy 2021; 235: 733–746.

Zhou Y, Zheng Y, Kan K, et al. Study on hydraulic char- acteristics of large vertical axial-flow pump

Zhou YS, Zhang H and Chen B. Influence of double- inlet design on the flow-head characteristics of axial-flow pump. J Hydrodyn 2021; 33: 763–772.

Yang F. Internal flow characteristics and hydraulic stabi- lity of low head pump. 1st ed. Beijing: China WaterPower Press, 2020, pp.17–62.

Li Y, Guo D, Fan Z, et al. Effects of different blade num- bers on radial exciting force of Lobe pump Rotor. Int J Fluid Machinery Syst 2020; 13: 281–291.

Wang D, Liu Z and Han W. Study on improving cavita- tion performance of centrifugal pump by perforation at the front cover plate. Int J Fluid Machinery Syst 2020; 13: 668–676.

Sheng X, Zhang D, Liu A, et al. Cavitation characteris- tics of tip leakage vortex and suction-side-perpendicular vortices in axial flow pump. Trans Chin Soc Agric Eng 2018; 34: 87–94.

Liu H, Liu M, Bai Y, et al. Grid convergence based on GCI for centrifugal pump. J Jiangsu Univ, Nat Sci Ed 2014; 35: 279–283.

Wang F. Flow Analysis method of pump and pump station. 1st ed. Beijing: China WaterPower Press, 2020.

Yan H, Liu M, Zhao W, et al. Influence of velocity circu- lation on hydraulic performance of large axial-flow pumps station. J Central South Univ 2016; 47: 2125–2132.

Liao W, Ji J, Peng LU, et al. Unsteady flow analysis of Francis turbine. J Mech Eng 2009; 45: 134–140.

Feng J, Wu H, Wu G, et al. Numerical simulation of pressure fluctuation in a Francis turbine at part load con- ditions with improved measures. J Hydraul Eng 2014; 45: